NANO LETTERS

pubs.acs.org/NanoLett Letter

All-Optical Manipulation of Magnetization in Ferromagnetic Thin Films Enhanced by Plasmonic Resonances

Feng Cheng, Chuangtang Wang, Zhaoxian Su, Xinjun Wang, Ziqiang Cai, Nian X. Sun, and Yongmin Liu*

Cite This: https://dx.doi.org/10.1021/acs.nanolett.0c02089 Read Online

ACCESS | Metrics & More | Article Recommendations | Supporting Information

ABSTRACT: In this paper, we report all-optical manipulation of magnetization in ferromagnetic Co/Pt thin films enhanced by plasmonic resonances. By annealing a thin Au layer, we fabricate large-area Au nanoislands on top of the Co/Pt magnetic thin films, which show plasmonic resonances around the wavelength of 606 nm. Using a customized magneto-optical Kerr effect setup, we experimentally observe an 18.5% decrease in the minimum laser power required to manipulate the magnetization, comparing the on- and off-resonance conditions. The results are in very good agreement with numerical simulations. Our research findings demonstrate the possibility to achieve an all-optical magnetic recording with low energy consumption, low cost, and high areal density by integrating plasmonic nanostructures with magnetic media.

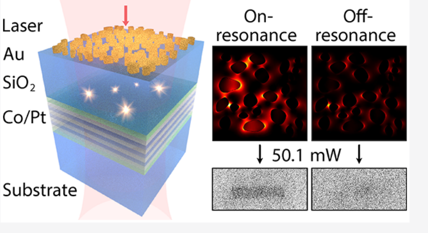

KEYWORDS: *plasmonics, all-optical manipulation, magnetization, ferromagnetic materials*

The rapid development of plasmonics over the last two decades has triggered a variety of research areas, such as biochemical sensing,[1,2] plasmon-enhanced energy harvesting,[3,4] plasmon-induced hot carrier generation,[5] plasmonic metamaterials,[6] magneto-plasmonics, and heat-assisted magnetic recording (HAMR) for data storage. In particular, magneto-plasmonics focus on the enhancement of magneto-optical effect by plasmonic nanostructures, such as nanodisks,[7−12] nanoholes,[13−19] and gratings.[20−28] On the other hand, we can utilize plasmonic nanoantennas,[29−34] resonant nanocavities,[35] or solid-immersion superoscillatory lens[36] to enhance the optothermal effect within the magnetic recording medium for HAMR technology. An external magnetic field is then applied to store data within the heated areas. So far, HAMR with an areal density up to petabyte per meter square has been realized.[30,31] The use of the plasmonic nanostructures has also been proposed in the research field of all-optical magnetization switching.[37−41] In this scheme, local magnetic fields delivered by a recording head are no longer needed. Instead, magnetization can be directly controlled by ultrafast laser pulses. Therefore, it is expected that the writing speed can be much faster than the current magnetic data storage technologies. In 2015, confined magnetic switching at the scale less than 100 nm was demonstrated in a system that gold antennas were integrated on top of a ferrimagnetic TbFeCo film, while the highly inhomogeneous nature of the switching process was also observed due to the heterogeneity of the TbFeCo film.[37] A recent publication reported the layer-selective all-optical magnetic recording assisted by surface plasmon polaritons, which would potentially increase the storage density of an opto-magnetic recording by a factor of at least two.[38] Besides the use of plasmonic nanostructures, researchers have also proposed other methods that can potentially increase the data storage density via azimuthally polarized vortex beams[42] and 3D light-induced magnetic holography.[43]

In addition to the areal density and writing speed, energy consumption is an equally important issue for data storage, which has not been explicitly explored in plasmon-mediated all-optical manipulation of magnetization. In this work, we present experimental observations of all-optical magnetization manipulation in ferromagnetic thin films enhanced by plasmonic resonances. Compared with ferrimagnetic materials, ferromagnetic materials generally have larger spin polarization and magnetic anisotropy, which are technically important for real applications, such as integrated magneto-optical memory, data storage, and data processing.[44] The plasmonic nanostructure adopted in our work is Au nanoislands, which can be easily fabricated with low cost and large area by annealing a thin Au layer under appropriate temperature and time conditions.[45−47] Such nanostructures have demonstrated applications in surface-enhanced Raman spectroscopy,[48] plasmon-enhanced photodetection,[49] and broadband absorbers.[50] It is shown that, by integrating Au nanoislands on top of magnetic media, we can locally enhance the electric fields

Received: May 16, 2020
Revised: July 26, 2020
Published: July 29, 2020

within the magnetic media, resulting in a lower laser threshold (about 18.5% decrease) to manipulate magnetization at the resonance wavelength of 606 nm in comparison with the off-resonance condition. We have performed full-wave simulations, which show a 17.0% enhancement of the electric field intensity in the Co/Pt thin films when comparing the on- and off-resonance wavelengths. This result quantitatively explains the observed reduction in the threshold. Due to their random geometries and distributions, the sample exhibits uniform plasmonic resonance, which is beneficial for practical applications.

Results and Discussion. *Sample Fabrication.* As illustrated in Figure 1a, the overall configuration of the sample

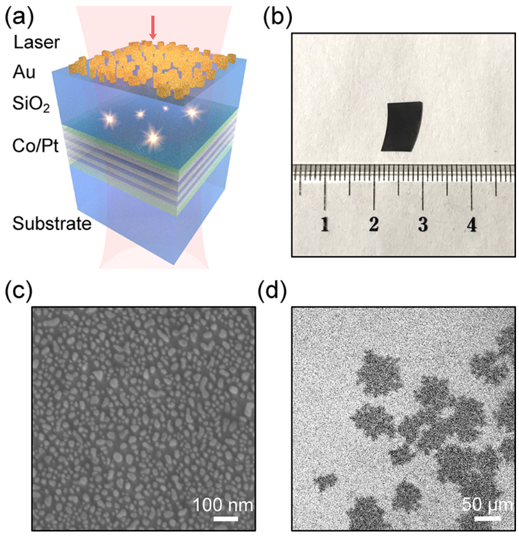

Figure 1. (a) Schematic view of the sample. A laser beams illuminates from the top side consisting of Au nanoislands. The electric field within the magnetic Co/Pt thin films is enhanced thanks to the plasmonic resonance of Au nanoislands, which reduces the minimum laser power to manipulate magnetization. (b) Photograph of the sample along with a ruler that has a unit length of 1 mm. (c) SEM image of the fabricated Au nanoislands. (d) MOKE microscopy image of the Co/Pt sample integrated with Au nanoislands, which clearly shows domains with out-of-plane magnetization.

can be considered as a metal (gold)-insulator (SiO_2)-metal (Co/Pt thin films) structure, which has been widely adopted to achieve perfect light absorption.[51,52] Figure 1b shows a photograph of the sample, indicating that our fabrication process can easily fabricate plasmonic nanostructures over a large scale yet with low cost, in comparison with conventional nanofabrication methods, such as electron beam lithography and focused ion beam (FIB) milling.[53−56] The scanning electron microscopy (SEM) image of the resulting Au nanoislands is presented in Figure 1c. The fabricated Au nanoislands are random in shapes and sizes, giving rise to the uniform and relatively broadband plasmonic resonance. The magnetic medium is Co/Pt ferromagnetic thin films, fabricated by DC magnetron sputtering onto a glass substrate at room temperature. The deposition was performed with an Ar pressure 3×10^{-3} Torr and a background pressure 10^{-7} Torr. The Co/Pt multilayer structure is Ta(3)/Pt(0.8)/$[Co(0.8)/Pt(0.8)]_3$/Ta(3), where the number in the bracket indicates the layer thickness in nanometers, and Ta serves as the seeding and cladding layer. The 20 nm SiO_2 spacing layer was fabricated by atomic layer deposition (ALD), and a thin layer of 5 nm Au was deposited by DC magnetron sputtering afterward. After fabrication, the sample was annealed in a chamber filled with Ar. The temperature was set to rise from 20 to 550 °C at a speed of 5 °C/min, held at 550 °C for 1 h, and then naturally cooled down to room temperature. Figure 1d presents the magneto-optical Kerr effect (MOKE) microscopy image of the sample. The black and white areas correspond to magnetic domains pointing downward and upward, respectively. When the laser illuminates the sample from the top side with the Au nanoislands, the electric field within the Co/Pt thin films will be enhanced at the plasmonic resonance wavelength of Au nanoislands. As a result, the minimum laser power required to manipulate magnetization in the magnetic medium will be reduced.

Sample Characterization. We have experimentally measured the transmittance spectra of the fabricated samples, including Co/Pt thin films with and without the Au nanoislands, by a spectrometer. The results are plotted in Figure 2a. Compared with the bare Co/Pt thin film, the Co/Pt

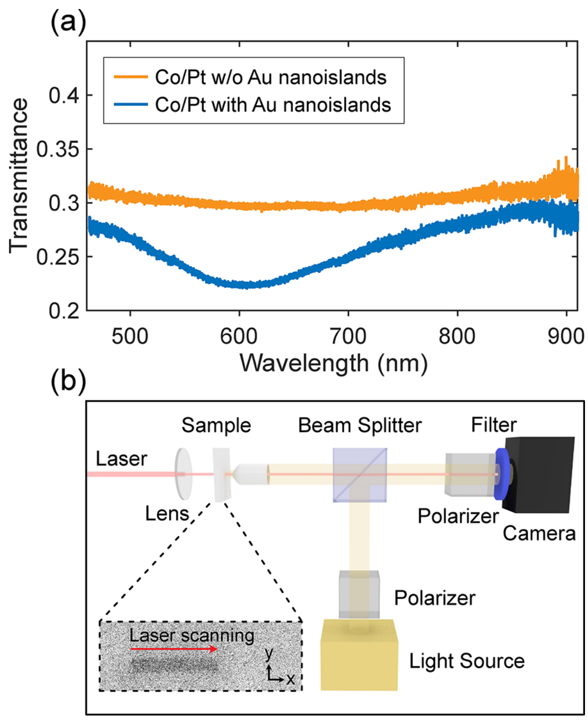

Figure 2. (a) Transmittance spectra of Co/Pt thin films with and without Au nanoislands. The results indicate the plasmonic resonance at 606 nm. (b) Illustration of the experimental setup. Inset: an example of the MOKE image after laser scanning.

film integrated with Au nanoislands shows a transmittance minimum at 606 nm, which indicates the plasmonic resonance at this wavelength. Therefore, we have chosen 606 nm, which is on-resonance, and 505 nm, which is off-resonance, to characterize the performances of all-optical magnetization manipulation.

Figure 2b illustrates the experimental setup. To manipulate the magnetization, we use a Ti:sapphire laser coupled with an optical parametric oscillator (OPO) from Coherent Inc., which allows for the tuning of the output wavelength. The repetition rate of the laser is 80 MHz, and the pulse width is 200 fs. The laser beam is focused on the sample by a lens. The magnetic domains are imaged by the home-built MOKE system, which

https://dx.doi.org/10.1021/acs.nanolett.0c02089
Nano Lett. XXXX, XXX, XXX−XXX

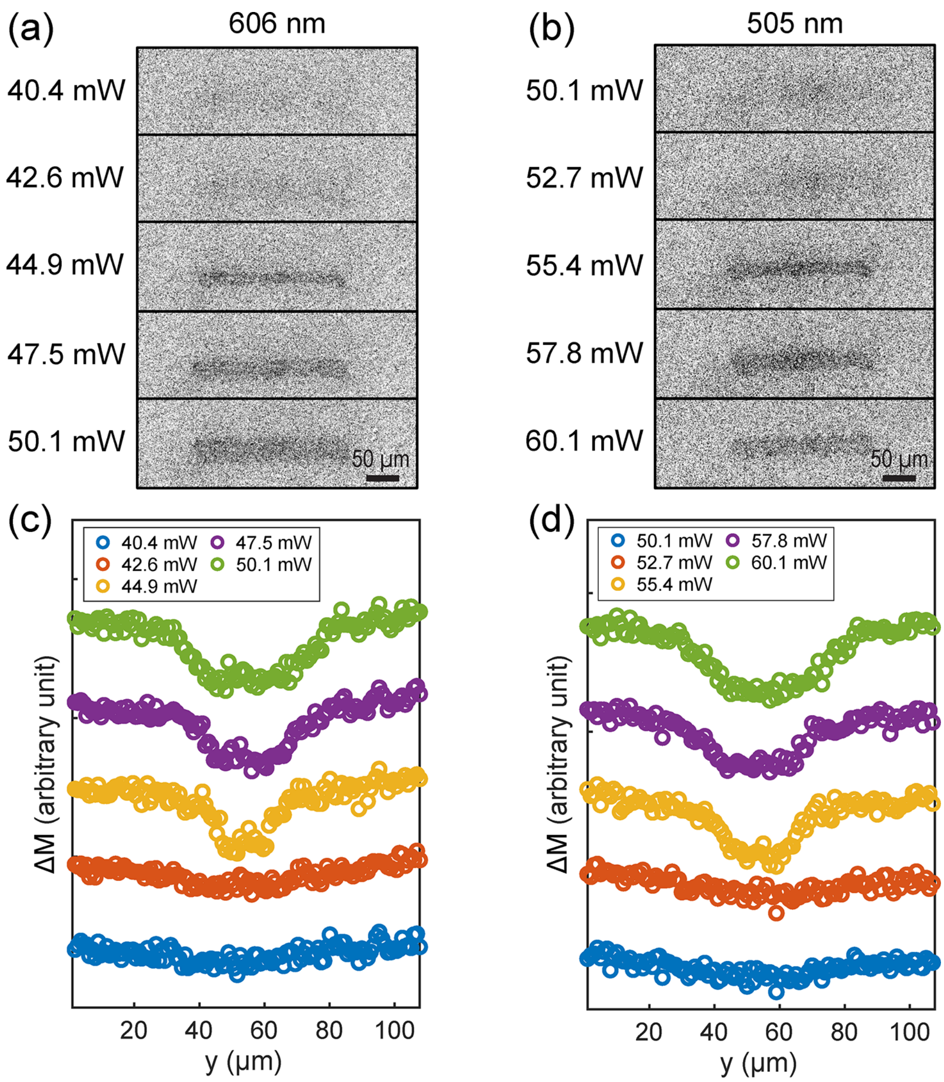

Figure 3. MOKE images of magnetization after laser scanning using different powers at the wavelength of (a) 606 nm and (b) 505 nm. (c, d) Cross-sectional plot of magnetization versus the *y*-axis at the two wavelengths, respectively.

Table 1. Threshold Power (in the Unit of mW) to Manipulate Magnetization Measured at Six Different Locations

test	1	2	3	4	5	6	mean	SD
606 nm	45.2	45.2	44.9	44.9	45.1	44.9	45.0	0.2
505 nm	55.4	54.8	54.9	55.3	55.4	55.1	55.2	0.3

consists of one white light source, one camera, and two Glan–Taylor polarizers. A short-pass filter with the cutoff wavelength of 500 nm (Thorlabs, FESH0500) is placed before the camera to block the high-intensity laser pulses while transmitting a large portion of the imaging white light. Depending on the magnetization orientation, linearly polarized light exhibits opposite polarization rotation angles that can be analyzed by a polarizer. Therefore, we can optically distinguish magnetizations pointing upward and downward, which show white and black contrasts in the MOKE image, respectively. The inset in Figure 2b shows an example of the MOKE image after scanning the laser on the Co/Pt thin films integrated with Au nanoislands. We define the laser scanning direction as the *x*-axis and the vertical direction as the *y*-axis for the subsequent analysis. It should be noted that all of the switched magnetization can be erased by external magnetic fields, unless the laser power is too high to damage the sample locally.

Plasmon-Enhanced Magnetization Manipulation. We have measured the minimum laser power required to manipulate magnetization in the Co/Pt with Au nanoislands at the on- and off-resonance wavelengths. Figure 3a,b presents the MOKE images after each laser scanning event for the two cases when the laser power gradually increases. At a 606 nm wavelength, which is the on-resonance condition, the magnetization manipulation can be achieved at 44.9 mW. While for 505 nm, which is the off-resonance condition, the magnetization manipulation is achieved at 55.4 mW. We estimated that the laser beam diameter at the wavelength of 606 and 505 nm was 28.9 and 24.1 μm, respectively. The fluence can be calculated by $F = \frac{P}{f\pi r^2}$ in which f = 80 MHz is the laser repetition rate, P denotes the laser power, and r is the laser beam radius. Therefore, the fluence thresholds are approximately 0.086 mJ/cm^2 and 0.15 mJ/cm^2 at the on-resonance

https://dx.doi.org/10.1021/acs.nanolett.0c02089
Nano Lett. XXXX, XXX, XXX−XXX

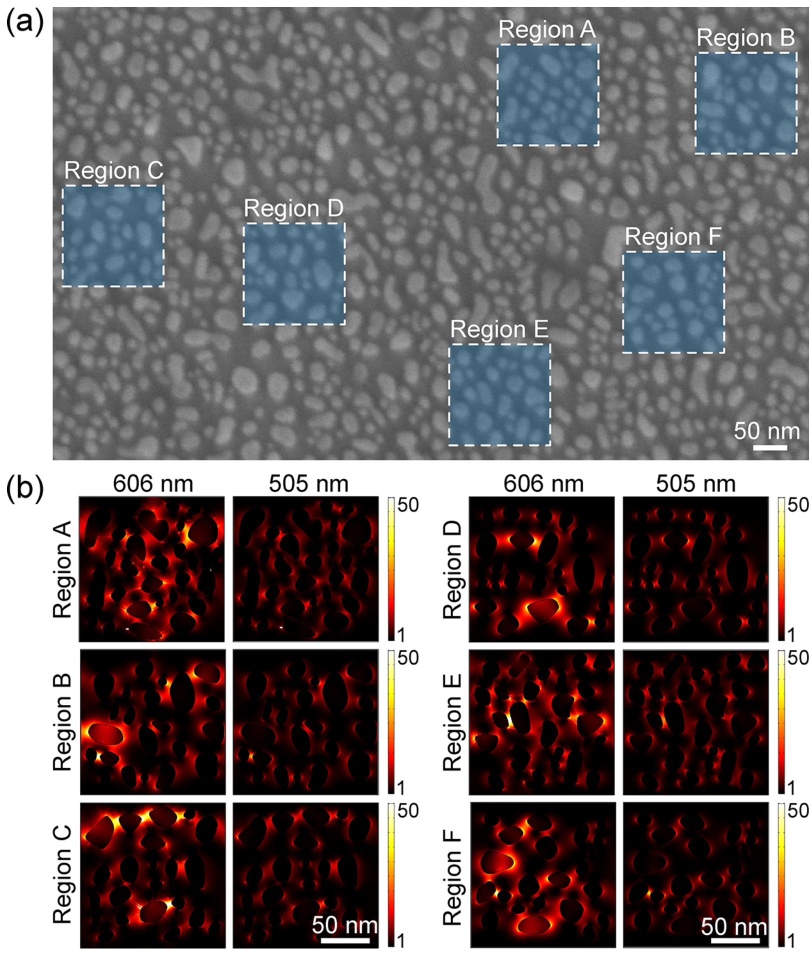

Figure 4. (a) SEM image of Au nanoislands, in which 6 regions (A−F), each in size of 150 nm × 150 nm, are randomly selected for the simulations. (b) Enhancement of electric field intensity in the middle plane of the Au nanoislands at the wavelength of 606 and 505 nm. A clear enhancement can be observed through the comparison between the on- and off-resonance wavelengths.

wavelength (606 nm) and off-resonance wavelength (505 nm), respectively.

To test the average performance of the sample, we have repeated these measurements at 6 randomly chosen locations on the sample, and similar results were observed. In Table 1, we present the observed threshold to manipulate magnetization for the 6 locations. As can be seen, at 606 nm, the averaged threshold is 45.0 mW with a standard deviation (SD) of 0.2 mW. At 505 nm wavelength, the averaged threshold is 55.2 mW with the standard deviation of 0.3 mW. The small standard deviation values indicate the uniform performances at different locations of our sample. From these experimental results, we calculate the percentage change for the magnetization manipulation threshold power as $(P_{\text{on-resonance}} - P_{\text{off-resonance}})/P_{\text{off-resonance}}$ = (45 mW − 55.2 mW)/55.2 mW = −18.5%, which indicates an 18.5% reduction.

We have conducted additional analyses to better qualify the observed phenomena. By integrating the value of pixels along the *x*-axis within the laser scanning regions, we plot the magnetization versus the *y*-axis. The cross-section of the magnetization at the wavelengths of 606 and 505 nm are shown in Figure 3c and 3d, respectively. For both wavelengths, no magnetization manipulation can be observed when the laser power is under the threshold value. If we increase the laser power to a value that is larger than the threshold, we observe the resulting magnetization as a trough in the plot, and the width of the trough becomes larger as the laser power increases. This is due to the Gaussian profile of the focused laser beam. When the laser power increases, there is a larger region that exceeds the threshold, resulting in a wider line after laser scanning events. The laser scanning experiments on bare Co/Pt thin films and the comparison with the samples integrated with Au nanoislands can be found in Sections 1 and 2 in the Supporting Information.

Modeling of the Plasmonic Enhancement Effect. We have simulated the local field distributions for the Co/Pt film integrated with Au nanoislands by commercial electromagnetic solver COMSOL Multiphysics. In order to obtain the averaged performance of the Au nanoislands, we randomly selected 6 regions as marked in Figure 4a, all in the size of 150 nm × 150 nm. After selection, the SEM images of Au nanoislands were vectorized and imported into COMSOL to reproduce their exact geometries. The thickness of the Au nanoislands was estimated to be 17 nm. The Co/Pt thin films and the Ta seed and capping layers were also included in the modeling. In Figure 4b, we present the enhancement of electric field intensity of the 6 regions in the middle plane of the Au layer at 606 and 505 nm. The enhancement is calculated by normalizing with the intensity of horizontally polarized incident light, which is set as 1 V^2/m^2. Note that all results were plotted with the same color bar so that we can compare the local enhancement directly. We can clearly see that, at the

https://dx.doi.org/10.1021/acs.nanolett.0c02089
Nano Lett. XXXX, XXX, XXX−XXX

Table 2. Averaged Electric Field Intensity in the Co/Pt Middle Plane for Regions A–F

region	A	B	C	D	E	F	mean	SD
606 nm	0.161	0.159	0.165	0.176	0.175	0.151	0.165	0.010
505 nm	0.136	0.138	0.141	0.146	0.142	0.140	0.141	0.003

resonance wavelength of 606 nm, the local fields in all of the 6 regions exhibit larger enhancement than those at the off-resonance wavelength. The simulated results show local hot spots generated by the plasmonic nanostructures, which give rise to a pronounced optothermal effect (see Section 3 in the Supporting Information). In addition, they can potentially be applied to achieve high-density magnetic storage.

To estimate the experimentally observed decrease of threshold power for magnetization manipulation, we have quantitatively calculated the averaged electric field intensity in the Co/Pt middle plane, which is normalized to the intensity of incident light for the 6 regions at the wavelength of 606 and 505 nm. The results are summarized in Table 2. We have calculated the averaged normalized electric field intensity for 606 nm, which is 0.165 with the standard deviation of 0.010, while, for 505 nm, it is 0.141 with the standard deviation of 0.003. As a result, we calculate the percentage increase as $(I_{\text{on-resonance}} - I_{\text{off-resonance}})/I_{\text{off-resonance}} = (0.165-0.141)/0.141 =$ 17.0% in the averaged normalized electric field intensity, which is consistent with the 18.5% decrease of the magnetization manipulation threshold observed in our experiment. It is expected that by pattering the plasmonic nanostructures into regular shapes, such as nanodisk and nanohole arrays,[57−59] we can further reduce the magnetization manipulation threshold at particular wavelengths. Our current simulation results of Au nanodisk arrays show that the maximum local intensity enhancement in the magnetic medium can reach up to 460% (see Section 4 in the Supporting Information).

In conclusion, in this work, we have proposed a method to reduce the energy consumption for magnetization manipulation by using the plasmonic resonance of Au nanoislands. The Au nanoislands are fabricated by annealing a thin Au layer and thus suitable for low-cost and mass production. We have experimentally measured an 18.5% reduction in the power required to manipulate magnetization. Full-wave simulations show an average enhancement of about 17.0% for the electric field intensity within the middle plane of magnetic media, which agrees well with the observed reduction of power threshold. Our results manifest the potential to achieve low-power and high-density all-optical magnetic data storage through the integration of plasmonic nanostructures.

ASSOCIATED CONTENT

Supporting Information

The Supporting Information is available free of charge at https://pubs.acs.org/doi/10.1021/acs.nanolett.0c02089.

Additional data and discussions including the all-optical manipulation of magnetization in the bare Co/Pt thin film and its comparison with the sample integrated with Au nanoislands, the simulation of the optothermal effect, and the design of Au nanodisk arrays to further enhance all-optical manipulation of magnetization (PDF)

AUTHOR INFORMATION

Corresponding Author

Yongmin Liu − *Department of Electrical and Computer Engineering and Department of Mechanical and Industrial Engineering, Northeastern University, Boston, Massachusetts 02115, United States;* orcid.org/0000-0003-1084-6651; Email: y.liu@northeastern.edu

Authors

Feng Cheng − *Department of Electrical and Computer Engineering, Northeastern University, Boston, Massachusetts 02115, United States*

Chuangtang Wang − *Department of Electrical and Computer Engineering, Northeastern University, Boston, Massachusetts 02115, United States*

Zhaoxian Su − *Department of Mechanical and Industrial Engineering, Northeastern University, Boston, Massachusetts 02115, United States*

Xinjun Wang − *Department of Electrical and Computer Engineering, Northeastern University, Boston, Massachusetts 02115, United States*

Ziqiang Cai − *Department of Electrical and Computer Engineering, Northeastern University, Boston, Massachusetts 02115, United States*

Nian X. Sun − *Department of Electrical and Computer Engineering, Northeastern University, Boston, Massachusetts 02115, United States;* orcid.org/0000-0002-3120-0094

Complete contact information is available at: https://pubs.acs.org/10.1021/acs.nanolett.0c02089

Notes

The authors declare no competing financial interest.

ACKNOWLEDGMENTS

Y.L. acknowledges the financial support of the National Science Foundation (DMR-1654192 and CBET-1931777). N.X.S. acknowledges the National Science Foundation Nanosystems ERC for Translational Applications of Nanoscale Multiferroic Systems (TANMS) led by the University of California, Los Angeles (EEC-1160504). We thank Dr. Vivek Jadhav and Prof. Meni Wanunu for the assistance in the ALD deposition of the SiO_2 dielectric layer. We also thank Dr. Zhiguang Wang for the help in the sample annealing process.

REFERENCES

(1) Stewart, M. E.; Anderton, C. R.; Thompson, L. B.; Maria, J.; Gray, S. K.; Rogers, J. A.; Nuzzo, R. G. Nanostructured Plasmonic Sensors. *Chem. Rev.* **2008**, *108* (2), 494−521.

(2) Anker, J. N.; Hall, W. P.; Lyandres, O.; Shah, N. C.; Zhao, J.; Van Duyne, R. P. Biosensing with Plasmonic Nanosensors. *Nat. Mater.* **2008**, *7* (6), 442−453.

(3) Atwater, H. A.; Polman, A. Plasmonics for Improved Photovoltaic Devices. *Nat. Mater.* **2010**, *9* (3), 205−213.

(4) Linic, S.; Christopher, P.; Ingram, D. B. Plasmonic-Metal Nanostructures for Efficient Conversion of Solar to Chemical Energy. *Nat. Mater.* **2011**, *10* (12), 911−921.

(5) Brongersma, M. L.; Halas, N. J.; Nordlander, P. Plasmon-Induced Hot Carrier Science and Technology. *Nat. Nanotechnol.* **2015**, *10* (1), 25−34.

(6) Yao, K.; Liu, Y. Plasmonic Metamaterials. *Nanotechnol. Rev.* **2014**, *3* (2), 177−210.

(7) Sepúlveda, B.; González-Díaz, J. B.; García-Martín, A.; Lechuga, L. M.; Armelles, G. Plasmon-Induced Magneto-Optical Activity in Nanosized Gold Disks. *Phys. Rev. Lett.* **2010**, *104* (14), 1.

(8) Barsukova, M. G.; Shorokhov, A. S.; Musorin, A. I.; Neshev, D. N.; Kivshar, Y. S.; Fedyanin, A. A. Magneto-Optical Response Enhanced by Mie Resonances in Nanoantennas. *ACS Photonics* **2017**, *4* (10), 2390−2395.

(9) Chen, L.; Gao, J.; Xia, W.; Zhang, S.; Tang, S.; Zhang, W.; Li, D.; Wu, X.; Du, Y. Tunable Fano Resonance and Magneto-Optical Response in Magnetoplasmonic Structure Fabricated by Pure Ferromagnetic Metals. *Phys. Rev. B: Condens. Matter Mater. Phys.* **2016**, *93* (21), 1.

(10) Kataja, M.; Hakala, T. K.; Julku, A.; Huttunen, M. J.; van Dijken, S.; Törmä, P. Surface Lattice Resonances and Magneto-Optical Response in Magnetic Nanoparticle Arrays. *Nat. Commun.* **2015**, *6*, 7072.

(11) Freire-Fernandez, F.; Kataja, M.; van Dijken, S. Surface-Plasmon-Polariton-Driven Narrow-Linewidth Magneto-Optics in Ni Nanodisk Arrays. *Nanophotonics* **2019**, *9* (1), 113.

(12) Freire-Fernández, F.; Mansell, R.; van Dijken, S. Magneto-plasmonic Properties of Perpendicularly Magnetized $[$Co/Pt$]
_{N}$ Nanodots. *Phys. Rev. B: Condens. Matter Mater. Phys.* **2020**, 1.

(13) Ctistis, G.; Papaioannou, E.; Patoka, P.; Gutek, J.; Fumagalli, P.; Giersig, M. Optical and Magnetic Properties of Hexagonal Arrays of Subwavelength Holes in Optically Thin Cobalt Films. *Nano Lett.* **2009**, *9* (1), 1−6.

(14) Papaioannou, E. T.; Kapaklis, V.; Melander, E.; Hjörvarsson, B.; Pappas, S. D.; Patoka, P.; Giersig, M.; Fumagalli, P.; Garcia-Martin, A.; Ctistis, G. Surface Plasmons and Magneto-Optic Activity in Hexagonal Ni Anti-Dot Arrays. *Opt. Express* **2011**, *19* (24), 23867−23877.

(15) Rollinger, M.; Thielen, P.; Melander, E.; Östman, E.; Kapaklis, V.; Obry, B.; Cinchetti, M.; García-Martín, A.; Aeschlimann, M.; Papaioannou, E. Th. Light Localization and Magneto-Optic Enhancement in Ni Antidot Arrays. *Nano Lett.* **2016**, *16* (4), 2432−2438.

(16) Papaioannou, E. T.; Fang, H.; Caballero, B.; Akinoglu, E. M.; Giersig, M.; García-Martín, A.; Fumagalli, P. Role of Interactions in the Magneto-Plasmonic Response at the Geometrical Threshold of Surface Continuity. *Opt. Express* **2017**, *25* (26), 32792−32799.

(17) Fang, H.; Caballero, B.; Akinoglu, E. M.; Papaioannou, E. Th.; García-Martín, A.; Cuevas, J. C.; Giersig, M.; Fumagalli, P. Observation of a Hole-Size-Dependent Energy Shift of the Surface-Plasmon Resonance in Ni Antidot Thin Films. *Appl. Phys. Lett.* **2015**, *106* (15), 153104.

(18) Caballero, B.; García-Martín, A.; Cuevas, J. C. Faraday Effect in Hybrid Magneto-Plasmonic Photonic Crystals. *Opt. Express* **2015**, *23* (17), 22238.

(19) Caballero, B.; García-Martín, A.; Cuevas, J. C. Hybrid Magnetoplasmonic Crystals Boost the Performance of Nanohole Arrays as Plasmonic Sensors. *ACS Photonics* **2016**, *3* (2), 203−208.

(20) Borovkova, O. V.; Hashim, H.; Kozhaev, M. A.; Dagesyan, S. A.; Chakravarty, A.; Levy, M.; Belotelov, V. I. TMOKE as Efficient Tool for the Magneto-Optic Analysis of Ultra-Thin Magnetic Films. *Appl. Phys. Lett.* **2018**, *112* (6), 063101.

(21) Khokhlov, N. E.; Prokopov, A. R.; Shaposhnikov, A. N.; Berzhansky, V. N.; Kozhaev, M. A.; Andreev, S. N.; Ravishankar, A. P.; Achanta, V. G.; Bykov, D. A.; Zvezdin, A. K.; Belotelov, V. I. Photonic Crystals with Plasmonic Patterns: Novel Type of the Heterostructures for Enhanced Magneto-Optical Activity. *J. Phys. D: Appl. Phys.* **2015**, *48* (9), 095001.

(22) Maksymov, I. S.; Hutomo, J.; Kostylev, M. Transverse Magneto-Optical Kerr Effect in Subwavelength Dielectric Gratings. *Opt. Express* **2014**, *22* (7), 8720.

(23) Chekhov, A. L.; Krutyanskiy, V. L.; Shaimanov, A. N.; Stognij, A. I.; Murzina, T. V. Wide Tunability of Magnetoplasmonic Crystals Due to Excitation of Multiple Waveguide and Plasmon Modes. *Opt. Express* **2014**, *22* (15), 17762.

(24) Chin, J. Y.; Steinle, T.; Wehlus, T.; Dregely, D.; Weiss, T.; Belotelov, V. I.; Stritzker, B.; Giessen, H. Nonreciprocal Plasmonics Enables Giant Enhancement of Thin-Film Faraday Rotation. *Nat. Commun.* **2013**, *4*, 1599.

(25) Kreilkamp, L. E.; Belotelov, V. I.; Chin, J. Y.; Neutzner, S.; Dregely, D.; Wehlus, T.; Akimov, I. A.; Bayer, M.; Stritzker, B.; Giessen, H. Waveguide-Plasmon Polaritons Enhance Transverse Magneto-Optical Kerr Effect. *Phys. Rev. X* **2013**, *3* (4), 041019.

(26) Pohl, M.; Kreilkamp, L. E.; Belotelov, V. I.; Akimov, I. A.; Kalish, A. N.; Khokhlov, N. E.; Yallapragada, V. J.; Gopal, A. V.; Nur-E-Alam, M.; Vasiliev, M.; Yakovlev, D. R.; Alameh, K.; Zvezdin, A. K.; Bayer, M. Tuning of the Transverse Magneto-Optical Kerr Effect in Magneto-Plasmonic Crystals. *New J. Phys.* **2013**, *15* (7), 075024.

(27) Grunin, A. A.; Zhdanov, A. G.; Ezhov, A. A.; Ganshina, E. A.; Fedyanin, A. A. Surface-Plasmon-Induced Enhancement of Magneto-Optical Kerr Effect in All-Nickel Subwavelength Nanogratings. *Appl. Phys. Lett.* **2010**, *97* (26), 261908.

(28) Belotelov, V. I.; Akimov, I. A.; Pohl, M.; Kotov, V. A.; Kasture, S.; Vengurlekar, A. S.; Gopal, A. V.; Yakovlev, D. R.; Zvezdin, A. K.; Bayer, M. Enhanced Magneto-Optical Effects in Magnetoplasmonic Crystals. *Nat. Nanotechnol.* **2011**, *6* (6), 370−376.

(29) Kryder, M.H.; Gage, E.C.; McDaniel, T.W.; Challener, W.A.; Rottmayer, R.E.; Ganping Ju; Yiao-Tee Hsia; Erden, M.F. Heat Assisted Magnetic Recording. *Proc. IEEE* **2008**, *96* (11), 1810−1835.

(30) Challener, W. A.; Peng, C.; Itagi, A. V.; Karns, D.; Peng, W.; Peng, Y.; Yang, X.; Zhu, X.; Gokemeijer, N. J.; Hsia, Y.-T.; Ju, G.; Rottmayer, R. E.; Seigler, M. A.; Gage, E. C. Heat-Assisted Magnetic Recording by a near-Field Transducer with Efficient Optical Energy Transfer. *Nat. Photonics* **2009**, *3* (4), 220−224.

(31) Stipe, B. C.; Strand, T. C.; Poon, C. C.; Balamane, H.; Boone, T. D.; Katine, J. A.; Li, J.-L.; Rawat, V.; Nemoto, H.; Hirotsune, A.; Hellwig, O.; Ruiz, R.; Dobisz, E.; Kercher, D. S.; Robertson, N.; Albrecht, T. R.; Terris, B. D. Magnetic Recording at 1.5 Pb m −2 Using an Integrated Plasmonic Antenna. *Nat. Photonics* **2010**, *4* (7), 484−488.

(32) Zhou, N.; Xu, X.; Hammack, A. T.; Stipe, B. C.; Gao, K.; Scholz, W.; Gage, E. C. Plasmonic Near-Field Transducer for Heat-Assisted Magnetic Recording. *Nanophotonics* **2014**, *3* (3), 141.

(33) Ju, G.; Peng, Y.; Chang, K.; Ding, Y.; Wu, A. Q.; Zhu, X.; Amini, H.; Klemmer, T. J.; Kubota, Y.; Gao, L.; Fan, Z.; Wang, K.; Rausch, T.; Subedi, P.; Kalarickal, S.; Dimitrov, D.; Ma, M.; Rea, C. J.; Karns, D. W.; Chen, X.; Dykes, J. W.; Seigler, M. A.; Gage, E.; Chantrell, R.; Thiele, J. High Density Heat Assisted Magnetic Recording Media and Advanced Characterization: Progress and Challenges. *In 2015 IEEE International Magnetics Conference (INTERMAG)* **2015**, 1−1.

(34) Kataja, M.; Freire-Fernández, F.; Witteveen, J. P.; Hakala, T. K.; Törmä, P.; van Dijken, S. Plasmon-Induced Demagnetization and Magnetic Switching in Nickel Nanoparticle Arrays. *Appl. Phys. Lett.* **2018**, *112* (7), 072406.

(35) Deng, C.; Song, H.; Parry, J.; Liu, Y.; He, S.; Xu, X.; Gan, Q.; Zeng, H. Nanocavity Induced Light Concentration for Energy Efficient Heat Assisted Magnetic Recording Media. *Nano Energy* **2018**, *50*, 750−755.

(36) Yuan, G.; Rogers, E. T. F.; Roy, T.; Shen, Z.; Zheludev, N. I. Flat Super-Oscillatory Lens for Heat-Assisted Magnetic Recording with Sub-50nm Resolution. *Opt. Express* **2014**, *22* (6), 6428−6437.

(37) Liu, T.-M.; Wang, T.; Reid, A. H.; Savoini, M.; Wu, X.; Koene, B.; Granitzka, P.; Graves, C. E.; Higley, D. J.; Chen, Z.; Razinskas, G.; Hantschmann, M.; Scherz, A.; Stohr, J.; Tsukamoto, A.; Hecht, B.; Kimel, A. V.; Kirilyuk, A.; Rasing, T.; Durr, H. A. Nanoscale Confinement of All-Optical Magnetic Switching in TbFeCo - Competition with Nanoscale Heterogeneity. *Nano Lett.* **2015**, *15* (10), 6862−6868.

https://dx.doi.org/10.1021/acs.nanolett.0c02089
Nano Lett. XXXX, XXX, XXX−XXX

(38) Ignatyeva, D. O.; Davies, C. S.; Sylgacheva, D. A.; Tsukamoto, A.; Yoshikawa, H.; Kapralov, P. O.; Kirilyuk, A.; Belotelov, V. I.; Kimel, A. V. Plasmonic Layer-Selective All-Optical Switching of Magnetization with Nanometer Resolution. *Nat. Commun.* **2019**, *10* (1), 1−7.

(39) Dutta, A.; Kildishev, A. V.; Shalaev, V. M.; Boltasseva, A.; Marinero, E. E. Surface-Plasmon Opto-Magnetic Field Enhancement for All-Optical Magnetization Switching. *Opt. Mater. Express* **2017**, *7* (12), 4316−4327.

(40) Koene, B.; Savoini, M.; Kimel, A. V.; Kirilyuk, A.; Rasing, T. Optical Energy Optimization at the Nanoscale by Near-Field Interference. *Appl. Phys. Lett.* **2012**, *101* (1), 013115.

(41) Ogut, E.; Kızıltas, G.; Sendur, K. Circularly Polarized Localized Near-Field Radiation at the Nanoscale. *Appl. Phys. B: Lasers Opt.* **2010**, *99* (1−2), 67−74.

(42) Jiang, Y.; Li, X.; Gu, M. Generation of Sub-Diffraction-Limited Pure Longitudinal Magnetization by the Inverse Faraday Effect by Tightly Focusing an Azimuthally Polarized Vortex Beam. *Opt. Lett.* **2013**, *38* (16), 2957.

(43) Hao, C.; Nie, Z.; Ye, H.; Li, H.; Luo, Y.; Feng, R.; Yu, X.; Wen, F.; Zhang, Y.; Yu, C.; Teng, J.; Luk'yanchuk, B.; Qiu, C.-W. Three-Dimensional Supercritical Resolved Light-Induced Magnetic Holography. *Science Advances* **2017**, *3* (10), No. e1701398.

(44) Lambert, C.-H.; Mangin, S.; Varaprasad, B. S. D. C. S.; Takahashi, Y. K.; Hehn, M.; Cinchetti, M.; Malinowski, G.; Hono, K.; Fainman, Y.; Aeschlimann, M.; Fullerton, E. E. All-Optical Control of Ferromagnetic Thin Films and Nanostructures. *Science* **2014**, *345* (6202), 1337−1340.

(45) Fujikawa, R.; Baryshev, A. V.; Kim, J.; Uchida, H.; Inoue, M. Contribution of the Surface Plasmon Resonance to Optical and Magneto-Optical Properties of a Bi:YIG-Au Nanostructure. *J. Appl. Phys.* **2008**, *103* (7), 07D301.

(46) Uchida, H.; Masuda, Y.; Fujikawa, R.; Baryshev, A. V.; Inoue, M. Large Enhancement of Faraday Rotation by Localized Surface Plasmon Resonance in Au Nanoparticles Embedded in Bi:YIG Film. *J. Magn. Magn. Mater.* **2009**, *321* (7), 843−845.

(47) Tkachuk, S.; Lang, G.; Krafft, C.; Rabin, O.; Mayergoyz, I. Plasmon Resonance Enhancement of Faraday Rotation in Thin Garnet Films. *J. Appl. Phys.* **2011**, *109* (7), 07B717.

(48) Zhang, N.; Liu, K.; Liu, Z.; Song, H.; Zeng, X.; Ji, D.; Cheney, A.; Jiang, S.; Gan, Q. Ultrabroadband Metasurface for Efficient Light Trapping and Localization: A Universal Surface-Enhanced Raman Spectroscopy Substrate for 'All ' Excitation Wavelengths. *Adv. Mater. Interfaces* **2015**, *2* (10), 1500142.

(49) Liu, Y.; Cheng, R.; Liao, L.; Zhou, H.; Bai, J.; Liu, G.; Liu, L.; Huang, Y.; Duan, X. Plasmon Resonance Enhanced Multicolour Photodetection by Graphene. *Nat. Commun.* **2011**, *2*, 579.

(50) Dereshgi, S. A.; Okyay, A. K. Large Area Compatible Broadband Superabsorber Surfaces in the VIS-NIR Spectrum Utilizing Metal-Insulator-Metal Stack and Plasmonic Nanoparticles. *Opt. Express* **2016**, *24* (16), 17644.

(51) Liu, N.; Mesch, M.; Weiss, T.; Hentschel, M.; Giessen, H. Infrared Perfect Absorber and Its Application As Plasmonic Sensor. *Nano Lett.* **2010**, *10* (7), 2342−2348.

(52) Li, Z.; Butun, S.; Aydin, K. Large-Area, Lithography-Free Super Absorbers and Color Filters at Visible Frequencies Using Ultrathin Metallic Films. *ACS Photonics* **2015**, *2* (2), 183−188.

(53) Kasani, S.; Curtin, K.; Wu, N. A Review of 2D and 3D Plasmonic Nanostructure Array Patterns: Fabrication, Light Management and Sensing Applications. *Nanophotonics* **2019**, *8* (12), 2065−2089.

(54) Broers, A. N.; Welland, M. E.; Gimzewski, J. K. Fabrication Limits of Electron Beam Lithography and of UV, X -Ray and Ion-Beam Lithographies. *Philosophical Transactions of the Royal Society of London. Series A: Physical and Engineering Sciences* **1995**, *353* (1703), 291−311.

(55) Gamo, K. Nanofabrication by FIB. *Microelectron. Eng.* **1996**, *32*, 159−171.

(56) Cui, X.; Qin, F.; Ruan, Q.; Zhuo, X.; Wang, J. Circular Gold Nanodisks with Synthetically Tunable Diameters and Thicknesses. *Adv. Funct. Mater.* **2018**, *28* (11), 1705516.

(57) Zheng, Y. B.; Juluri, B. K.; Kiraly, B.; Huang, T. J. Ordered Au Nanodisk and Nanohole Arrays: Fabrication and Applications. *J. Nanotechnol. Eng. Med.* **2010**, *1* (3), 031011.

(58) Wang, J.; Duan, G.; Li, Y.; Liu, G.; Cai, W. Wet Etching-Assisted Colloidal Lithography: A General Strategy toward Nanodisk and Nanohole Arrays on Arbitrary Substrates. *ACS Appl. Mater. Interfaces* **2014**, *6* (12), 9207−9213.

(59) Cui, X.; Qin, F.; Ruan, Q.; Zhuo, X.; Wang, J. Circular Gold Nanodisks with Synthetically Tunable Diameters and Thicknesses. *Adv. Funct. Mater.* **2018**, *28* (11), 1705516.